

Atomic layer etching of ferroelectric hafnium zirconium oxide thin films enables giant tunneling electroresistance

Cite as: Appl. Phys. Lett. **120**, 122901 (2022); doi: [10.1063/5.0084636](https://doi.org/10.1063/5.0084636)

Submitted: 8 January 2022 · Accepted: 8 March 2022 ·

Published Online: 25 March 2022



View Online



Export Citation



CrossMark

M. Hoffmann,^{1,a),b)}  J. A. Murdzek,²  S. M. George,²  S. Slesazek,³  U. Schroeder,³  and T. Mikolajick^{3,4} 

AFFILIATIONS

¹Department of Electrical Engineering and Computer Sciences, University of California, Berkeley, California 94720, USA

²Department of Chemistry, University of Colorado, Boulder, Colorado 80309-0215, USA

³NaMLab gGmbH, Dresden 01187, Germany

⁴Chair of Nanoelectronics, TU Dresden, Dresden 01187, Germany

^{a)}Author to whom correspondence should be addressed: hoffmann@berkeley.edu

^{b)}This research was performed while M. Hoffmann was at NaMLab gGmbH, Dresden 01187, Germany.

ABSTRACT

The ferroelectric properties of hafnium oxide and zirconium oxide based thin films are promising for applications in low power electronics, such as ultra-thin ferroelectric tunneling devices. However, the amount of ferroelectric phase in the film depends on their polycrystalline morphology, which changes with film thickness. Therefore, controlling the film thickness without changing the ferroelectric properties has remained challenging. Here, we propose the use of thermal atomic layer etching to decouple the ferroelectric phase stabilization from the film thickness. First, the ferroelectric phase fraction is maximized by crystallizing the film at an optimized film thickness. Subsequently, the ferroelectric film thickness is reduced to the desired range by atomic layer etching. We demonstrate the feasibility of this approach for a ferroelectric hafnium zirconium oxide film of 10 nm initial thickness, which we integrate into a double-layer ferroelectric tunnel junction. The atomic layer etch rate of ferroelectric hafnium zirconium oxide using HF and dimethylaluminum chloride is found to be ~ 0.2 Å/cycle. Although the ferroelectric phase persists after atomic layer etching, the etching increases the surface roughness. For applications in ferroelectric tunnel junctions, we show that atomic layer etching of ferroelectric hafnium zirconium oxide can improve the read current by more than a factor of 200, while at the same time reducing the read voltage by 43%. The resulting tunneling electroresistance of about 2500 is the highest reported so far for polycrystalline hafnium zirconium oxide-based materials.

Published under an exclusive license by AIP Publishing. <https://doi.org/10.1063/5.0084636>

The recently discovered class of fluorite-structure ferroelectrics based on HfO_2 and ZrO_2 (Refs. 1 and 2) is promising for a broad range of applications in electronics, such as nonvolatile memories,^{3,4} nanoscale transistors,^{5,6} and neuromorphic computing.^{7,8} The main advantages of fluorite-structure ferroelectrics for such applications are their full compatibility with current semiconductor manufacturing technologies⁹ as well as their thickness scalability down to 1 nm.¹⁰ Conformal growth on high aspect ratio substrates is possible due to the availability of mature atomic layer deposition (ALD) processes.¹¹ The solid solution of hafnium zirconium oxide ($\text{Hf}_{1-x}\text{Zr}_x\text{O}_2$, HZO) is particularly promising for applications due to its low crystallization temperature and the broad composition range that exhibits ferroelectricity.²

However, most fluorite-structure ferroelectric thin films are polycrystalline and consist of a mixture of polar and non-polar

phases,^{12,13} which is detrimental, for example, for applications in nonvolatile memories.¹⁴ The competing phases are the ferroelectric orthorhombic $\text{Pca}2_1$ phase, which energetically lies between the non-polar tetragonal $\text{P}4_2/\text{nmc}$ phase and the non-polar monoclinic $\text{P}2_1/\text{c}$ phase.¹² The ideal film thickness for the highest orthorhombic phase fraction is often observed around 10 nm, depending on the film composition.¹³ The reason for this ideal film thickness is that the as-deposited films are typically amorphous. A subsequent post-deposition or post-metallization anneal is then needed to crystallize the film. Since the average grain size of the film after annealing depends on the film thickness, so do the fractions of polar and non-polar phases.^{15,16} Therefore, thicker films (larger grain size) tend to be more monoclinic while thinner films (smaller grain size) tend to have more tetragonal and amorphous

phase fractions.^{12,13,15,17} Typically, the tetragonal phase is found close to the electrode interfaces.¹⁸

For many applications of fluorite-structure ferroelectrics, being able to adjust the film thickness without reducing the amount of ferroelectric phase fraction would be beneficial. For example, ferroelectric tunnel junctions (FTJs) rely on a nondestructive readout of the ferroelectric polarization by measuring the tunneling current through the device.^{19–23} This current increases exponentially as the film thickness of the tunneling layer is reduced and depends upon the polarization direction. Therefore, to achieve a high read current in an FTJ, the ferroelectric should be generally as thin as possible, without compromising reliability.^{24,25} At the same time, the ferroelectric film should ideally be fully orthorhombic, such that the difference in read current between the two polarization directions is maximized.^{25–27} Here, we propose to achieve this by preparing a ferroelectric film in the thickness range where the orthorhombic phase fraction is maximum (~ 10 nm) and subsequently reducing its thickness by a careful etching process.²⁸

Recently, polycrystalline HfO_2 , ZrO_2 , and HZO films were etched by using thermal atomic layer etching (ALE) processes.²⁹ ALE is an etching technique consisting of at least two sequential, self-limiting surface reactions,³⁰ which is of interest, e.g., for the manufacturing of advanced semiconductor devices.³¹ Similar to the sub-monolayer thickness control of ALD techniques for film growth, thermal ALE enables isotropic etching of a material with sub-monolayer precision.³² Here, we apply a thermal ALE process using fluorination and ligand-exchange reactions, which have been described in detail elsewhere.^{29,33} We show that such ALE processes can also be applied for etching polycrystalline fluorite-structure ferroelectrics, which presents an opportunity to increase the read-current and tunneling electroresistance in FTJ devices.

A simplified schematic of the process flow is shown in Fig. 1. First, metal-ferroelectric-metal (MFM) capacitors were fabricated on p-Si (100) with a native SiO_2 layer. TiN bottom electrodes of 12 nm thickness were reactively sputtered in a BESTEC physical vapor deposition tool at room temperature. Subsequently, 10 nm HZO ($\text{Hf}_{0.5}\text{Zr}_{0.5}\text{O}_2$) was grown by atomic layer deposition in a Roth & Rau ALD tool at 280 °C using TEMAHf , $\text{CpZr}[\text{N}(\text{CH}_3)_2]_3$, and O_3 as the oxygen source. The total number of ALD cycles for HZO was fixed at 100, resulting in ~ 10 nm thick films. Then, 12 nm thick TiN top electrodes were deposited with the same process used for the bottom electrodes. After top electrode deposition, a post-metallization anneal at 600 °C for 20 s in N_2 was performed to crystallize the $\text{Hf}_{0.5}\text{Zr}_{0.5}\text{O}_2$ layer predominantly into the ferroelectric orthorhombic $\text{Pca}2_1$ phase.

Subsequently, the TiN top electrode was removed by an SC-1 etch (NH_4OH , H_2O_2 , and H_2O solution). Before atomic layer etching (ALE) of the ferroelectric HZO layer, the thin TiON layer, which forms during the annealing step at the HZO/TiN top interface, was removed by a 10 min soak in 10% HF. ALE of HZO was carried out in a viscous flow reactor at 250 °C using HF as the fluorination reactant and dimethylaluminum chloride (DMAC) as the metal precursor for ligand-exchange. The details of the ALE process and reactor are described elsewhere.²⁹ Different samples were subjected to 50, 100, 200, or 300 ALE cycles of HF/DMAC to determine the etch rate per ALE cycle.

In between the ALE cycles, the etched HZO thickness was monitored using spectroscopic ellipsometry (SE) and x-ray reflectometry

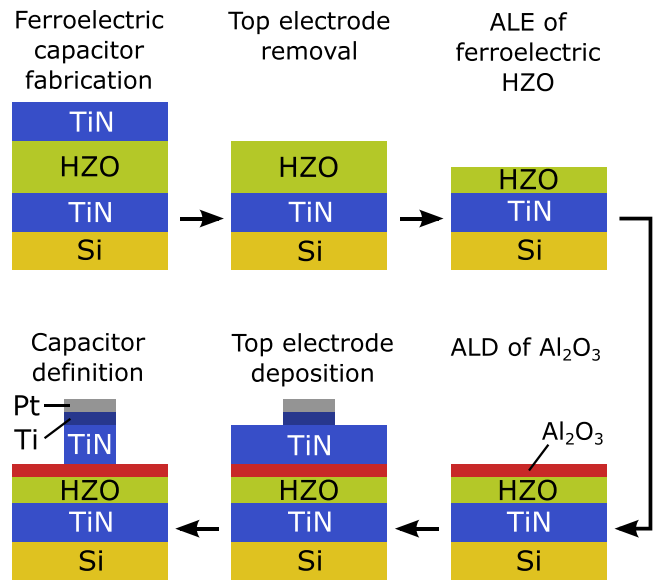


FIG. 1. Simplified process flow for ferroelectric tunnel junction fabrication including thermal atomic layer etching (ALE) of the ferroelectric hafnium zirconium oxide (HZO). ALD: Atomic layer deposition.

(XRR) as shown in Fig. 2(a). The ALE etch rate of HZO was found to be $\sim 0.2 \text{ \AA/cycle}$ at 250 °C. This is comparable to previous reports on mixed tetragonal/monoclinic polycrystalline HZO films, where an etch rate of 0.16 \AA/cycle was observed using HF/DMAC.²⁹ When excluding the 300 cycle data points in Fig. 2(a), which have the largest relative uncertainty, the etch rate will be comparable to the previous data.²⁹ This indicates that the presence of the spontaneous ferroelectric polarization does not seem to have a strong effect on the ALE process of HZO. However, the ALE process does affect the surface roughness of the ferroelectric HZO film as was investigated by atomic force microscopy (AFM). The surface roughness of the ferroelectric HZO films (after TiN top electrode and TiON removal) is plotted in Fig. 2(b), showing a general trend of increasing surface roughness with number of ALE cycles. Figure 2(c) shows the AFM scan for the 10 nm ferroelectric HZO film before ALE. Despite its polycrystalline morphology, the surface roughness is relatively smooth. However, after 200 ALE cycles, the surface roughness increases as can be seen in Fig. 2(d).

The AFM images suggest that some regions of the polycrystalline film are etched faster than others. Previous observations found that amorphous HZO is etched more than four times faster than polycrystalline HZO using HF/DMAC.²⁹ Similar etching results for amorphous and crystalline material were also obtained for HfO_2 , ZrO_2 , and Al_2O_3 .^{29,34} Thus, small amorphous or defect rich regions, such as grain boundaries, might be etched faster than the ferroelectric grains themselves, leading to increasing surface roughness. Grains of different size, crystal phase, or orientation might also have different effective etch rates contributing to this effect. Potentially, different etching behavior between grains could be used to selectively etch only grains of certain sizes, orientations, or crystallographic phase.

Grazing-incidence x-ray diffraction (GIXRD) measurements were carried out before and after ALE (10 and 7.4 nm HZO thickness,

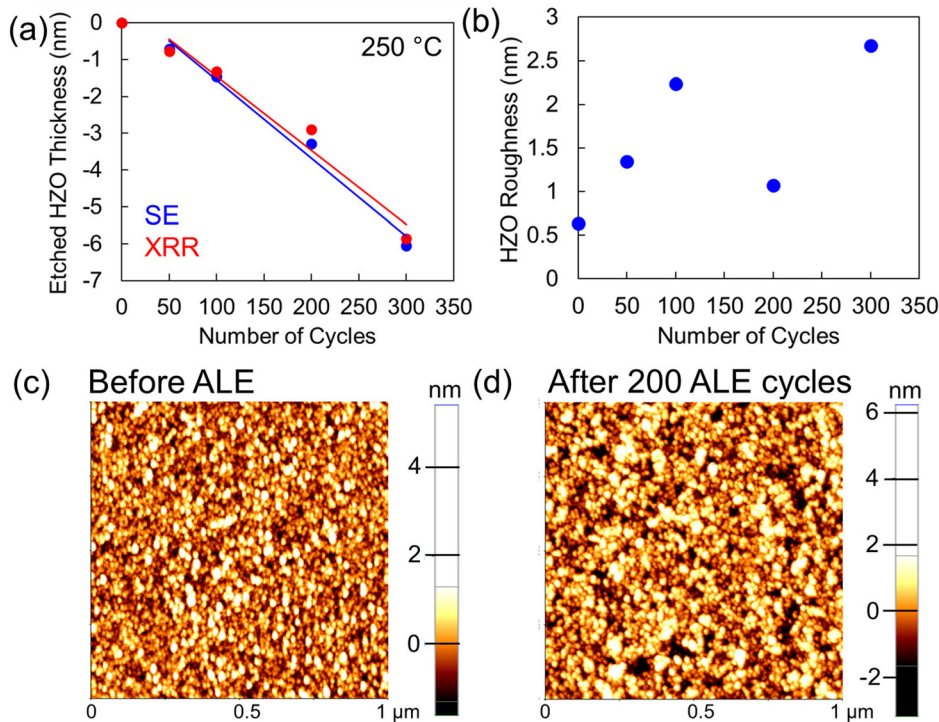


FIG. 2. (a) Etched hafnium zirconium oxide (HZO) thickness as a function of atomic layer etching (ALE) cycles measured by spectroscopic ellipsometry (SE) and x-ray reflectometry (XRR). (b) HZO film roughness determined by atomic force microscopy (AFM) as a function of the number of ALE cycles. AFM scans (c) before ALE and (d) after 200 cycles of ALE.

respectively). As can be seen in Fig. 3, before ALE, the films exhibit a GIXRD pattern consistent with the orthorhombic/tetragonal phases, which are difficult to distinguish from GIXRD alone. Monoclinic phase fractions are not detected. Electrical characteristics showing predominantly ferroelectric behavior in 10 nm HZO films fabricated under the same experimental conditions as reported here, can be found elsewhere.³⁵ These electrical data suggest that the HZO films are mostly orthorhombic with only minor tetragonal phase fractions.

According to the GIXRD data in Fig. 3, the orthorhombic peaks are still present after ALE, but their magnitude is reduced, which is expected for a thinner film. However, some of the peaks show a stronger reduction in magnitude after ALE than others. These findings might indicate different etch rates between the different crystal orientations of the orthorhombic grains. Nevertheless, due to the increased surface roughness after ALE, any quantitative evaluation will be difficult. Furthermore, it was previously reported that fully tetragonal ZrO_2 and amorphous HZO films exhibit ALE etch rates of 0.82 and 0.69 Å/cycle, respectively,²⁹ which is much higher than the 0.2 Å/cycle observed for our mostly orthorhombic films. This suggests that any initial tetragonal or amorphous phase fractions in our films will be etched faster than the orthorhombic phase using this ALE process. Thus, some of the peaks that overlap for the tetragonal and orthorhombic phase (e.g., at $\sim 30^\circ$) might show a stronger reduction since the tetragonal phase is completely etched away. This is consistent with the slight shift of the 30° peak toward lower angles [see Fig. 3(b)], which indicates a reduction of the tetragonal phase compared to the orthorhombic phase. A similar reduction of the tetragonal GIXRD peaks is observed when comparing the 7.4 nm ALE sample with a 7.7 nm HZO sample that was processed in a similar way but without

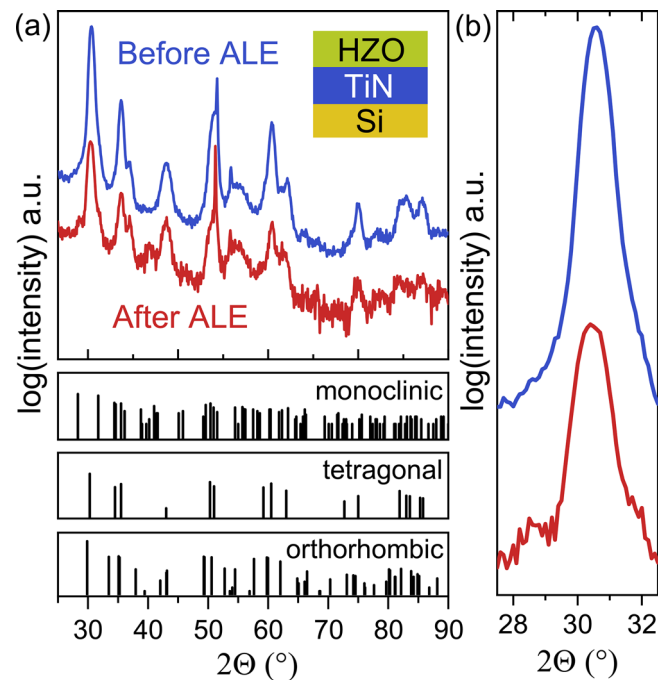


FIG. 3. Grazing incidence x-ray diffraction patterns of hafnium zirconium oxide (HZO) before and after thermal atomic layer etching (ALE), corresponding to 10 and 7.4 nm HZO thickness, respectively. Reference patterns for the monoclinic $\text{P}2_1/c$ phase, the tetragonal $\text{P}4_2/nmc$ phase, and the orthorhombic $\text{P}ca2_1$ phase are given below. (b) shows a zoom-in on the peak at 30° from (a).

ALE, see the [supplementary material](#). Therefore, ALE could help to effectively increase the orthorhombic phase fraction by a faster etching of any non-orthorhombic regions in the film. In future studies, local characterization of samples after ALE, e.g., using piezo-response force microscopy, could give more insights into these inhomogeneous etching effects.

After ALE of multiple samples with different ALE cycles, to create double-layer FTJs, Al_2O_3 was grown by ALD in the same Roth & Rau ALD tool used for the HZO at 280°C using TMA and O_3 as the oxygen source. According to XRR, a 2.9 nm Al_2O_3 thin film was grown on the remaining HZO layer by using 22 ALD cycles of Al_2O_3 . Afterward, 12 nm thick TiN top electrodes were deposited with the same process as described before. To create the contact pads, 10 nm of Ti and 30 nm of Pt were evaporated onto the TiN top electrode using a shadow mask. These evaporated Ti/Pt dots served as a hard mask during the final SC-1 etch of the TiN top electrode.

Figure 4 shows the electrical characterization results of the TiN/HZO/ Al_2O_3 /TiN samples before and after ALE using a Keithley 4200 SCS with RPM remote amplifier. Current-voltage curves were acquired with a Source Measure Unit (SMU) dual voltage sweep with a step size of 100 mV. We note that samples, which were etched to an HZO thickness below 4 nm (XRR), were completely shorted and are, therefore, not shown here. In Fig. 4(a), the inverse small-signal capacitance at a frequency of 10 kHz and zero DC bias is shown as a function of the HZO thickness measured with XRR. The data point at 10 nm corresponds to the sample without ALE. From the linear fit, we can extract a relative permittivity of Al_2O_3 and HZO from the slope and intercept, respectively, assuming both layers are electrically in series. When also considering the TiN interface capacitance in series to the

other capacitances,³⁵ we obtain ~ 8.6 and 38 for Al_2O_3 and HZO, respectively, which is consistent with values found in the literature.

Additionally, current-voltage characteristics were measured as shown in Fig. 4(b), with the positive voltage applied to the bottom electrode. As a general trend, increasing current with reduced HZO thickness is observed as expected. The samples with 10, 7.4, and 6.2 nm HZO show typical hysteresis as observed in other double-layer FTJ devices.²⁷ However, the thinnest sample with 4.9 nm HZO behaved differently, with orders of magnitude larger current than the other samples (up to 1 A/cm^2). For this 4.9 nm sample, the markedly different behavior might be related to a complete etching of the HZO in some regions of the film, which could result in a combination of filamentary and ferroelectric switching.³⁶ For the well behaved FTJ devices (6.2, 7.4, and 10 nm), we can see that the difference of the current levels for positive voltages (applied to the bottom electrode) is increasing for decreasing HZO thickness.

Figure 4(c) shows both the ON- and OFF-currents (I_{ON} and I_{OFF}) for positive voltages, where the $I_{\text{ON}}/I_{\text{OFF}}$ ratio is maximized. One can see that I_{OFF} is largely unaffected by the reduction of the HZO thickness by ALE, while I_{ON} strongly increases by more than a factor of 200 going from 10 to 6.2 nm HZO. Considering the band diagram of a double-layer FTJ, this behavior is expected: In the OFF-state, the current path is blocked by most of the HZO/ Al_2O_3 double-layer, such that direct tunneling and Fowler-Nordheim (FN) tunneling contributions to the total current should be negligible. I_{OFF} is likely dominated by trap-assisted tunneling currents, which will have a much weaker dependence on the HZO thickness. On the other hand, in the ON-state, FN tunneling through the Al_2O_3 layer is likely dominating, since the unscreened polarization at the HZO/ Al_2O_3 interface will pull

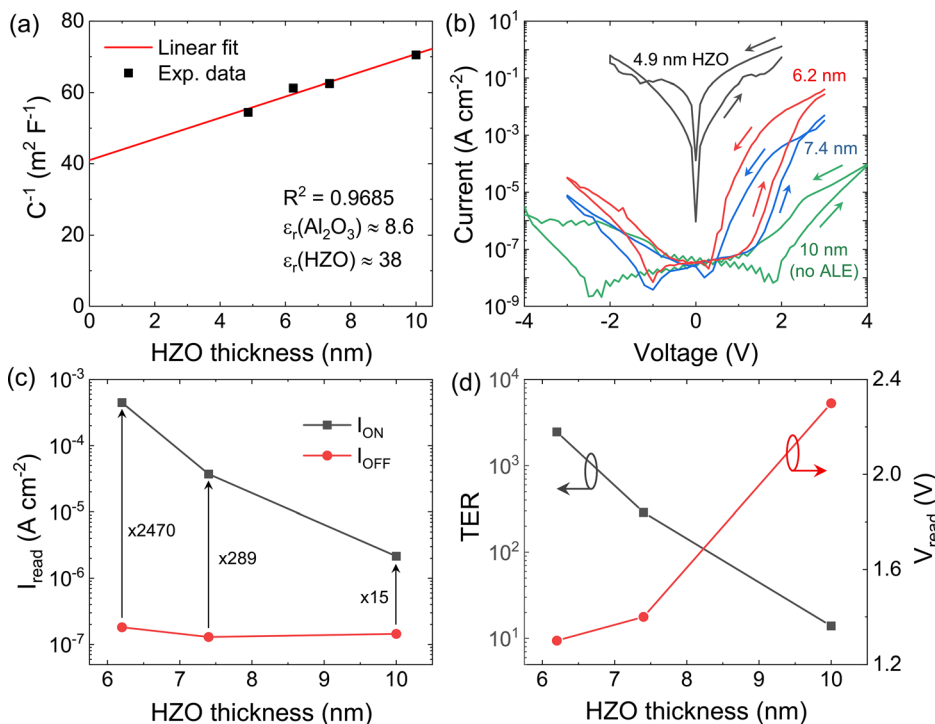


FIG. 4. (a) Inverse capacitance as a function of hafnium zirconium oxide (HZO) thickness for HZO/ Al_2O_3 capacitors. (b) Current-voltage characteristics for samples with and without atomic layer etching (ALE) of HZO. The voltage is applied to the bottom electrode. (c) Tunnel junction read current in the ON- and OFF-state as a function of the HZO thickness. (d) Tunneling electroresistance (TER) and read voltage (V_{read}) as a function of the HZO thickness.

down the Al_2O_3 conduction band edge at this interface.^{37,38} In this case, a strong HZO thickness dependence of I_{ON} is expected. In contrast, for a potential filamentary switching mechanism in HZO, we would expect a linear increase in I_{ON} with reduced HZO thickness since the resistance of the filament would be proportional to its length. Furthermore, I_{ON} for filamentary switching devices is typically orders of magnitude larger ($>1 \text{ A cm}^{-2}$) compared to our 6.2 and 7.4 nm samples. Therefore, our results cannot be explained by such a filamentary mechanism.

Finally, Fig. 4(d) shows the maximum tunneling electroresistance [TER = $(I_{\text{ON}} - I_{\text{OFF}})/I_{\text{OFF}}$] for each HZO thickness, as well as the corresponding read voltage V_{read} , which is defined as the voltage at which this maximum TER occurs. With the decreasing HZO thickness, the TER increases from 14 (for 10 nm) to 288 (for 7.4 nm) and then to 2469 (for 6.2 nm). At the same time, V_{read} decreases from 2.3 to 1.4 V and then to 1.3 V, respectively. This shows that ALE of ferroelectric HZO can be used to improve the ON-current of the double-layer FTJs by more than a factor of 200 without degrading I_{OFF} , while at the same time reducing the read voltage by 43%. The giant TER observed for the device with the 6.2 nm HZO thickness is the largest value reported in the literature for polycrystalline fluorite-structure based FTJs.³⁹ A comparison of the key metrics of various reported FTJs can be found in Table I.

In summary, we have proposed and demonstrated an approach to reduce the thickness of ferroelectric films of fluorite structure, without changing the phase composition, by using thermal ALE. By first crystallizing the film in the thickness range where the ferroelectric phase fraction is maximized and then etching the film with ALE, we decouple the process of phase stabilization from the film thickness. We showed that for thermal ALE using HF/DMAC, we obtain an etch rate of $\sim 0.2 \text{ \AA/cycle}$ for mainly orthorhombic HZO. While the

TABLE I. Benchmarking reported HZO based ferroelectric tunnel junctions (FTJs). t_{FE} is the ferroelectric film thickness, I_{ON} and I_{OFF} are the current densities in the ON- and OFF-states, respectively, and V_{read} is the read voltage.

FTJ stack	t_{FE} (nm)	$I_{\text{ON}}/I_{\text{OFF}}$	I_{ON} (A cm^{-2})	V_{read} (V)	Ref.
Pt/HZO/TiN	2.8	16	5.7×10^{-6}	0.2	19
Ge/ Al_2O_3 /HZO/TiN	8.4	14	1.7×10^{-5}	1.4	20
	12	32	2.5×10^{-5}	2	
TiN/ Al_2O_3 /HZO/TiN	8	20	9.5×10^{-6}	2	40
	12	14	4.5×10^{-6}	2	
Si/HZO/ Al_2O_3 /Ti/Au	12	6	6×10^{-5}	2	38
unknown	3	13	0.1	3	21
Pt/HZO/TiN	9	20	...	0.1	22
Si/ SiO_2 /HfO _x /TiN	6	33	0.004	2	23
Si/ SiO_2 /HZO/W	1	200	10	0.25	24
Si/ SiO_2 /HZO/TiN	4	31	1×10^{-3}	0.2	25
Ge/HZO/TiN	8	21	...	0.2	26
TiN/ Al_2O_3 /HZO/TaN	10	100	4×10^{-6}	0.9	27
W/HZO/MoS ₂ /org-W	4.5	1000	1×10^{-3}	0.8	39
TiN/ Al_2O_3 /HZO/TiN	7.4	289	4×10^{-5}	1.4	This
	6.2	2470	4.5×10^{-4}	1.3	work

ferroelectric phase persists after ALE according to GIXRD and electrical measurements, the surface roughness of the film increases after ALE, which might contribute to the large increase in the current in the ON-state. We demonstrate that ALE of ferroelectric HZO can be used to substantially improve the read current, TER and read voltage of double-layer FTJs.

See the [supplementary material](#) for a comparison of GIXRD data of HZO films with similar thickness, processed with and without ALE as well as preliminary reliability data of the FTJ with 6.2 nm HZO thickness.

This work was financially supported out of the State budget approved by the delegates of the Saxon State Parliament.

AUTHOR DECLARATIONS

Conflict of Interest

The authors have no conflicts to disclose.

DATA AVAILABILITY

The data that support the findings of this study are available from the corresponding author upon reasonable request.

REFERENCES

- T. S. Börscke, J. Müller, D. Bräuhaus, U. Schröder, and U. Böttger, "Ferroelectricity in hafnium oxide thin films," *Appl. Phys. Lett.* **99**, 102903 (2011).
- J. Müller, T. S. Börscke, U. Schröder, S. Mueller, D. Bräuhaus, U. Böttger, L. Frey, and T. Mikolajick, "Ferroelectricity in simple binary ZrO_2 and HfO_2 ," *Nano Lett.* **12**, 4318–4323 (2012).
- M. H. Park, Y. H. Lee, T. Mikolajick, U. Schroeder, and C. S. Hwang, "Review and perspective on ferroelectric HfO₂-based thin films for memory applications," *MRS Bull.* **8**, 795–808 (2018).
- T. Mikolajick, U. Schroeder, and S. Slesazek, "The past, the present, and the future of ferroelectric memories," *IEEE Trans. Electron Devices* **67**, 1434–1443 (2020).
- A. I. Khan, A. Keshavarzi, and S. Datta, "The future of ferroelectric field-effect transistor technology," *Nat. Electron.* **3**, 588–597 (2020).
- M. Hoffmann, S. Slesazek, and T. Mikolajick, "Progress and future prospects of negative capacitance electronics: A materials perspective," *APL Mater.* **9**, 020902 (2021).
- B. Max, M. Hoffmann, H. Mulaosmanovic, S. Slesazek, and T. Mikolajick, "Hafnia-based double-layer ferroelectric tunnel junctions as artificial synapses for neuromorphic computing," *ACS Appl. Electron. Mater.* **2**, 4023–4033 (2020).
- S. Yu, J. Hur, Y.-C. Luo, W. Shim, G. Choe, and P. Wang, "Ferroelectric HfO₂-based synaptic devices: Recent trends and prospects," *Semicond. Sci. Technol.* **36**, 104001 (2021).
- U. Schroeder, S. Mueller, J. Mueller, E. Yurchuk, D. Martin, C. Adelman, T. Schloesser, R. v. Bentum, and T. Mikolajick, "Hafnium oxide based CMOS compatible ferroelectric materials," *ECS J. Solid State Sci. Technol.* **2**, N69 (2013).
- S. Cheema, D. Kwon, N. Shanker, R. d. Reis, S.-L. Hsu, J. Xiao, H. Zhang, R. Wagner, A. Datar, M. R. McCarter, C. R. Serrao, A. K. Yadav, G. Karbasian, C.-H. Hsu, A. J. Tan, L.-C. Wang, V. Thakare, X. Zhang, A. Mehta, E. Karapetrova, R. V. Chopdekar, P. Shafer, E. Arenholz, C. Hu, R. Proksch, R. Ramesh, J. Ciston, and S. Salahuddin, "Enhanced ferroelectricity in ultrathin films grown directly on silicon," *Nature* **580**, 478–482 (2020).
- J. Müller, T. S. Börscke, S. Müller, E. Yurchuk, P. Polakowski, J. Paul, D. Martin, T. Schenk, K. Khullar, A. Kersch, W. Weinreich, S. Riedel, K. Seidel, A. Kumar, T. M. Arruda, S. V. Kalinin, T. Schlösser, R. Boschke, R. v. Bentum, U. Schröder, and T. Mikolajick, "Ferroelectric hafnium oxide: A CMOS-compatible and

- highly scalable approach to future ferroelectric memories,” in IEEE International Electron Devices Meeting (IEDM), Washington, DC, 2013.
- ¹²M. Hoffmann, U. Schroeder, T. Schenk, T. Shimizu, H. Funakubo, O. Sakata, D. Pohl, M. Drescher, C. Adelman, R. Materlik, A. Kersch, and T. Mikolajick, “Stabilizing the ferroelectric phase in doped hafnium oxide,” *J. Appl. Phys.* **118**, 072006 (2015).
- ¹³U. Schroeder, C. S. Hwang, and H. Funakubo, *Ferroelectricity in Doped Hafnium Oxide: Materials, Properties and Devices* (Woodhead Publishing, 2019).
- ¹⁴F. Mehmood, M. Hoffmann, P. D. Lomenzo, C. Richter, M. Materano, T. Mikolajick, and U. Schroeder, “Bulk depolarization fields as a major contributor to the ferroelectric reliability performance in lanthanum doped $\text{Hf}_{0.5}\text{Zr}_{0.5}\text{O}_2$ capacitors,” *Adv. Mater. Interfaces* **6**, 1901180 (2019).
- ¹⁵H. J. Kim, M. H. Park, Y. J. Kim, Y. H. Lee, W. Jeon, T. Gwon, T. Moon, K. D. Kim, and C. S. Hwang, “Grain size engineering for ferroelectric $\text{Hf}_{0.5}\text{Zr}_{0.5}\text{O}_2$ films by an insertion of Al_2O_3 interlayer,” *Appl. Phys. Lett.* **105**, 192903 (2014).
- ¹⁶T. Mittmann, F. P. G. Fengler, C. Richter, M. H. Park, T. Mikolajick, and U. Schroeder, “Optimizing process conditions for improved $\text{Hf}_{1-x}\text{Zr}_x\text{O}_2$ ferroelectric capacitor performance,” *Microelectron. Eng.* **178**, 48–51 (2017).
- ¹⁷X. Tian, S. Shibayama, T. Nishimura, T. Yajima, S. Migita, and A. Toriumi, “Evolution of ferroelectric HfO_2 in ultrathin region down to 3 nm,” *Appl. Phys. Lett.* **112**, 102902 (2018).
- ¹⁸E. D. Grimley, T. Schenk, X. Sang, M. Pešić, U. Schroeder, T. Mikolajick, and J. M. LeBeau, “Structural changes underlying field-cycling phenomena in ferroelectric HfO_2 thin films,” *Adv. Electron. Mater.* **2**(9), 1600173 (2016).
- ¹⁹F. Ambriz-Vargas, G. Kolhatkar, M. Broyer, A. Hadj-Youssef, R. Nouar, A. Sarkissian, R. Thomas, C. Gomez-Yáñez, M. A. Gauthier, and A. Ruediger, “A complementary metal oxide semiconductor process-compatible ferroelectric tunnel junction,” *ACS Appl. Mater. Interfaces* **9**, 13262–13268 (2017).
- ²⁰A. Shekhawat, G. Walters, N. Yang, J. Guo, T. Nishida, and S. Moghaddam, “Data retention and low voltage operation of $\text{Al}_2\text{O}_3/\text{Hf}_{0.5}\text{Zr}_{0.5}\text{O}_2$ based ferroelectric tunnel junctions,” *Nanotechnology* **31**, 39LT01 (2020).
- ²¹S. Fujii, Y. Kamimuta, T. Ino, Y. Nakasaki, R. Takaiishi, and M. Saitoh, “First demonstration and performance improvement of ferroelectric HfO_2 -based resistive switch with low operation current and intrinsic diode property,” in IEEE Symposium on VLSI Technology, Honolulu, 2016.
- ²²L. Chen, T.-Y. Wang, Y.-W. Dai, M.-Y. Cha, H. Zhu, Q.-Q. Sun, S.-J. Ding, P. Zhou, L. Chua, and D. W. Zhang, “Ultra-low power $\text{Hf}_{0.5}\text{Zr}_{0.5}\text{O}_2$ based ferroelectric tunnel junction synapses for hardware neural network applications,” *Nanoscale* **10**, 15826–15833 (2018).
- ²³K. K. Min, J. Yu, Y. Kim, J.-H. Lee, D. Kwon, and B.-G. Park, “Interlayer engineering for enhanced ferroelectric tunnel junction operations in HfO_x -based metal-ferroelectric-insulator-semiconductor stack,” *Nanotechnology* **32**, 495203 (2021).
- ²⁴S. S. Cheema, N. Shanker, C.-H. Hsu, A. Datar, J. Bae, D. Kwon, and S. Salahuddin, “One nanometer HfO_2 -based ferroelectric tunnel junctions on silicon,” *Adv. Electron. Mater.* (published online, 2021).
- ²⁵M. Kobayashi, Y. Tagawa, F. Mo, T. Saraya, and T. Hiramoto, “Ferroelectric HfO_2 tunnel junction memory with high TER and multi-level operation featuring metal replacement process,” *J. Electron Devices Soc.* **7**, 134–139 (2019).
- ²⁶Y. Goh and S. Jeon, “Enhanced tunneling electroresistance effects in HfZrO -based ferroelectric tunnel junctions by high-pressure nitrogen annealing,” *Appl. Phys. Lett.* **113**, 052905 (2018).
- ²⁷K.-Y. Hsiang, C.-Y. Liao, J.-H. Liu, J.-F. Wang, S.-H. Chiang, S.-H. Chang, F.-C. Hsieh, H. Liang, C.-Y. Lin, Z.-F. Lou, T.-H. Hou, C. W. Liu, and M. H. Lee, “Bilayer-based antiferroelectric HfZrO_2 tunneling junction with high tunneling electroresistance and multilevel nonvolatile memory,” *IEEE Electron Device Lett.* **42**, 1464–1467 (2021).
- ²⁸J. C. Gertsch, E. Sortino, V. M. Bright, and S. M. George, “Deposit and etch-back approach for ultrathin Al_2O_3 films with low pinhole density using atomic layer deposition and atomic layer etching,” *J. Vacuum Sci. Technol. A* **39**, 062602 (2021).
- ²⁹J. A. Murdzek and S. M. George, “Effect of crystallinity on thermal atomic layer etching of hafnium oxide, zirconium oxide, and hafnium zirconium oxide,” *J. Vacuum Sci. Technol. A* **38**, 022608 (2020).
- ³⁰A. Fischer, A. Rutzahn, S. M. George, and T. Lill, “Thermal atomic layer etching: A review,” *J. Vacuum Sci. Technol. A* **39**, 030801 (2021).
- ³¹K. J. Kanarik, T. Lill, E. A. Hudson, S. Sriraman, S. Tan, J. Marks, V. Vahedi, and R. A. Gottscho, “Overview of atomic layer etching in the semiconductor industry,” *J. Vacuum Sci. Technol. A* **33**, 020802 (2015).
- ³²T. Faraz, F. Roozeboom, H. C. M. Knoops, and W. M. M. Kessels, “Atomic layer etching: What can we learn from atomic layer deposition?,” *ECS J. Solid State Sci. Technol.* **4**, N5023 (2015).
- ³³S. M. George, “Mechanisms of thermal atomic layer etching,” *Acc. Chem. Res.* **53**, 1151–1160 (2020).
- ³⁴J. A. Murdzek, A. Rajashekhar, R. S. Makala, and S. M. George, “Thermal atomic layer etching of amorphous and crystalline Al_2O_3 films,” *J. Vacuum Sci. Technol. A* **39**, 042602 (2021).
- ³⁵M. Hoffmann, M. Gui, S. Slesazek, R. Fontanini, M. Segatto, D. Esseni, and T. Mikolajick, “Intrinsic nature of negative capacitance in multidomain $\text{Hf}_{0.5}\text{Zr}_{0.5}\text{O}_2$ -based ferroelectric/dielectric heterostructures,” *Adv. Funct. Mater.* **32**, 2108494 (2021).
- ³⁶B. Max, M. Pešić, S. Slesazek, and T. Mikolajick, “Interplay between ferroelectric and resistive switching in doped crystalline HfO_2 ,” *J. Appl. Phys.* **123**, 134102 (2018).
- ³⁷H. Li, P. Chang, G. Du, J. Kang, and X. Liu, “Impact of interfacial layer on the switching characteristics of HZO-based ferroelectric tunnel junction,” in International Symposium on VLSI Technology, Systems and Applications (VLSI-TSA), Hsinchu, 2021.
- ³⁸H. Ryu, H. Wu, F. Rao, and W. Zhu, “Ferroelectric tunneling junctions based on aluminum oxide/zirconium-doped hafnium oxide for neuromorphic computing,” *Sci. Rep.* **9**, 20383 (2019).
- ³⁹P. Chaudhary, P. Buragohain, M. Kozodaev, S. Zarubin, V. Mikheev, A. Chouprik, A. Lipatov, A. Sinitiskii, A. Zenkevich, and A. Gruverman, “Electroresistance effect in MoS_2 - $\text{Hf}_{0.5}\text{Zr}_{0.5}\text{O}_2$ heterojunctions,” *Appl. Phys. Lett.* **118**, 083106 (2021).
- ⁴⁰B. Max, M. Hoffmann, S. Slesazek, and T. Mikolajick, “Retention characteristics of $\text{Hf}_{0.5}\text{Zr}_{0.5}\text{O}_2$ -based ferroelectric tunnel junctions,” in IEEE 11th International Memory Workshop (IMW), Monterey, CA, 2019.